International Journal of Fluid Dynamics (2001) **Vol 5**, Article 4, 41-58
Available online at: http://elecpress.monash.edu.au/ijfd

The Simulation of Vortex Dynamics downstream of a Plate Separator using a Vortex-Finite Element Method

Iraj Mortazavi[a] & André Giovannini[b]
[a] *Mathématiques Appliquées de Bordeaux, UMR CNRS 5466, Université Bordeaux 1, 351 Cours de La Libération, 33405 Talence Cedex, France*
[b] *Institut de Mécanique des Fluides de Toulouse, UMR CNRS 5502, Université Toulouse, Avenue de Professeur Camille Soula, 31400 Toulouse Cedex, France*

Keywords: Numerical simulation, Vortex method, Channel flow, Plate separator, Vorticity dynamics, Flow visualisation

The dynamics of vorticity in a bluff-body geometry for an incompressible, unsteady, plane, high Reynolds number flow is studied using a vortex method. The numerical scheme corresponds to a hybrid of the Random Vortex Method (RVM) and Finite-Element Method (FEM). A Vortex-In-Cell post-processing technique provides integral (streamfunction) and primitive (velocity) variables. A predictor-corrector pressure field computation algorithm is applied to study the pressure field evolution. Various techniques of instantaneous visualisation, as well particle frequency analyses and average field tests are applied to characterise such flow behaviour. Dynamic visualisation techniques focussing on the mechanisms of formation and transport of eddy structures represent a powerful tool for the analysis of such complex flows. The effect of the thickness of the bluff-body and of different inlet velocity ratios is studied to assess the evolution and interaction of vortical structures downstream of the bluff-body's mixing zone.

1. INTRODUCTION

Vortex methods are applied to simulate 2D incompressible steady and more particularly unsteady fluid flow in a wide range of Reynolds number regimes. The first successful presentation of vortex methods, containing a non-singular discretisation of the Navier-Stokes equations was proposed by Chorin (1973) and named the Random Vortex Method. Later, Chorin modified his method to account for wall boundary conditions, and named it the Vortex Sheet Method (Chorin 1978). During the last decade, different classes of vortex methods have been proposed to solve the Navier-Stokes equations with a random or deterministic diffusion operator.

Vortex methods deal with non-primitive variables and their main well-known advantage is related to the optimised computational efficiency arising from the fact that vortex elements are accounted for only in regions on non-zero vorticity, and partially from the fact that, dealing directly with vorticity, we have immediate physical insights on the behaviour

in vortical sub-domains such as those where separated flow structures occur. Hence the essential feature of this class of simulations methods is related to its unsteady nature and its suitability to vortex dynamics studies.

Vortex methods have been used to monitor different complex flows. Ghoniem et al. (1982) have studied qualitatively a high Reynolds number flow in a backward-facing step problem. Later, Ghoniem & Gagnon (1987) presented a complete study of backward-facing step laminar flows. The study of this geometry has further been extended to the case of the transitional regime by Sethian & Ghoniem (1988), and completed with precise quantitative studies by Gagnon & Giovannini (1993) for larger Reynolds numbers. Ghoniem & Najm (1991), and Choi et al. (1988) used the RVM to study moderate and high Reynolds number fluid flows in short and long cavities. Ghoniem & Najm focussed extensively on the vortex shedding properties in these kinds of geometries. The capability of these techniques to focus on vortical sub-regions makes them an efficient tool to study separated flows and mixing zones. Several authors have therefore been interested in this subject. Ghoniem & Ng (1987) analyzed the dynamics of a mixing zone downstream of a flat plate while Blot et al. (1989) simulated the flow pattern around and downstream of a rectangular bluff-body inside a channel, modelling the geometry of a vortex flow-meter. Gagnon & Huang (1993) studied the flow behaviour inside channels with and without lateral injection and finally, Martins & Ghoniem (1993) simulated the non-reacting flow in a bluff-body burner. In this latter work, the authors gave a general overview of vortex interactions in axisymmetrical mixing zones. Other applications of these schemes can be found in combustion (Sethian 1984), biomechanics (McCracken & Peskin 1980), and in the simulation of wind flow over buildings (Summers et al. 1985).

Many of the above mentioned works have validated the RVM for moderate (Ghoniem et al. 1982, Ghoniem & Gagnon 1987, Choi et al. 1988) and high (Gagnon et al. 1993, Najm & Ghoniem 1991, Ghoniem & Ng 1987, Blot et al. 1989, Martins & Ghoniem 1993) Reynolds number flows, validating them against experiments or other numerical methods. These high Reynolds number validation studies confirm the capability of vortex methods to simulate accurately complex flows. Furthermore, the numerical convergence of this method for spatial and time discretisation parameters is extensively explored separately (Ghoniem & Gagnon 1987, Sethian & Ghoniem 1988, Mortazavi 1997, Mortazavi et al. 1996).

In the present work, the RVM is used to describe the strong dynamics of the flow due to the interaction between an inner jet and an external flow separated by two symmetrical flat plates. The flow is unsteady, two-dimensional (plane) and incompressible. The study is oriented toward the characterisation of the formation and transport of eddy structures in the flow domain. The interaction and mixing of the two entry flows downstream of the separator imposes an interesting and complicated dynamics to the flow behaviour. Both entry flows have uniform profiles (the normal component of the velocity is zero). Because of the symmetry, only half of the whole geometry is considered here (Figure 1). It will be observed that, in spite of the random nature of turbulence, the creation of vortical structures downstream of the obstacle, their mutual interactions just before the separation from the obstacle and their transport by the main flow follows a quasi-coherent logic which can be analyzed by instantaneous observations of the fluid patterns.

The first objective will be to study the effect of the plate thickness on the flow map. A thick ($h_b = 0.45$, $H/h = 0.5$) and a thin ($h_b = 0.25$, $H/h = 0.3$) obstacle are compared for different mean and instantaneous simulation results. Here h_b is the bluff-body thickness

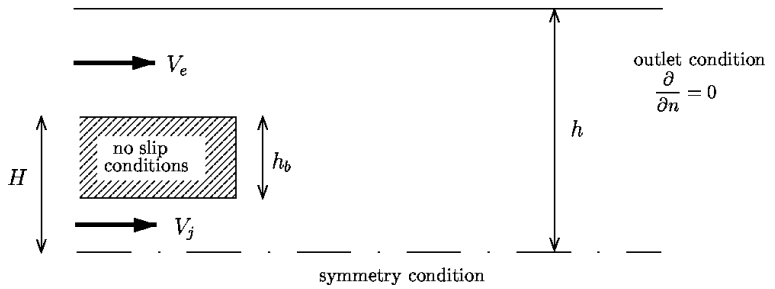

Figure 1. Geometry of flow domain showing boundary conditions

and H/h corresponds to the ratio of the obstacle distance from the axis to the channel half-height. The generation of two opposite-sign vorticity layers on the two edges of the separation leads to instabilities, deformation of vortical structures, merging and mixing. In order to increase the topological richness of the vortex pattern analyzed, we choose to create a maximum competition between the jet effect and the outer wake effect, by forcing the velocity ratio of the two streams to be equal to unity (Figure 1). For the thin obstacle, the eddy structures are smaller and contain fewer vortex elements. This aspect is quite important to allow the vortex structures to preserve their initial form for a large period of time; also, it permits one to simplify the vortex agglomerations, following the theoretical point vortex hypothesis. However, for the thick obstacle case the eddies' evolution is quite slow and their size is larger than in the previous case. These large eddies easily lose their initial form and are transformed into smaller vortical structures, interacting and mixing during the beginning of their transport. These observations are confirmed by frequency and Strouhal number analyses.

The second objective of this work concerns the effect of the entry velocity ratio on the vortex formation and transport. For this study, two velocity ratios are compared: $V_j/V_e = 0.5$ and $V_j/V_e = 2.0$, where V_e and V_j correspond respectively to the external flow velocity and the jet velocity. Numerical results show that events are dominated by the flow having the larger velocity and consequently larger absolute vorticity.

Qualitative and quantitative methods of numerical flow visualisation, spectral and monitoring point analyses and average streamlines and velocity fields are applied to complete this study. The flow is visualised using temporal sequences of fields of various quantities. Furthermore, the evolution of the number of vortex elements and circulation values with time are plotted. These plots provide a clear understanding of the eddies' time and space behaviour.

2. NUMERICAL METHOD

The Random Vortex Method is a numerical technique to solve for the incompressible, 2D, unsteady Navier-Stokes equations converted to a rotational non-primitive formulation. The equations to be solved are the Poisson Equation

$$\nabla^2 \Psi = -\omega, \tag{1}$$

and the Vorticity Transport Equation (VTE)

$$\frac{\partial \omega}{\partial t} + \mathbf{u} \cdot \nabla \omega = \frac{1}{Re} \nabla^2 \omega, \tag{2}$$

associated with their boundary conditions. Here Ψ is the stream function, w the non-zero component of the vorticity, $\mathbf{u}$ the velocity vector and Re the Reynolds number. To discretise the vorticity, the computational domain is divided into two regions: the "interior" region and the numerical boundary region. In the interior region the vorticity is discretised using vortex "blobs" (Chorin 1973), whereas in the boundary domain vortex "sheets" are used (Chorin 1978). The VTE is solved by a two-step fractional-step method: the first step corresponding to the convection and the second one to the diffusion.

2.1. THE MATHEMATICAL MODEL IN NON-PRIMITIVE FORMULATION (VELOCITY VERSUS VORTICITY)

Classically the solution of the Poisson Equation using the free boundary domain Green's function leads to

$$\mathbf{u}_\omega(\mathbf{x}, t) = \int_D \mathbf{K}(\mathbf{x} - \mathbf{x}')\omega(\mathbf{x}')\, d\mathbf{x}', \tag{3}$$

where $\mathbf{K}(\mathbf{x}) = (1/2\pi)(y, -x)/r^2)$ is the integral kernel of the Poisson equation.

In a bounded domain and for an inviscid flow, the solution is searched as: $\mathbf{u} = \mathbf{u}_p + \mathbf{u}_\omega$; $\mathbf{u}_p$ being the irrotational component of the velocity.

$\mathbf{u}_p = \nabla\phi$ and

$$\nabla^2 \phi = 0, \tag{4}$$

where ϕ is the potential function. The boundary conditions associated with equation (4) are such that $\mathbf{u}$ satisfies global the boundary condition $\mathbf{u} \cdot \mathbf{n} = 0$ (or $\nabla\phi \cdot \mathbf{n} = \mathbf{u}_p \cdot \mathbf{n} = -\mathbf{u}_\omega \cdot \mathbf{n}$) on the wall; $\mathbf{u}$ is imposed at the entrance of the domain and $\nabla \mathbf{u} \cdot \mathbf{n} = 0$ at the exit ($\mathbf{n}$ is the normal unit vector to the wall).

For a viscous flow the wall condition is $\mathbf{u} = \mathbf{0}$; more details about the implementation of the no-slip conditions will be given in the next section.

2.2. THE VORTICITY TRANSPORT EQUATION

Equation (2) is solved by a method using two fractional steps. First, we solve the convective part of this equation:

$$\frac{D\omega}{Dt} = 0 \tag{5}$$

and

$$\frac{d\mathbf{x}}{dt} = \mathbf{u}. \tag{6}$$

The trajectory of a fluid particle defined by

$$\mathbf{x}(\alpha, t) = \mathbf{x}(\alpha, 0) + \int_0^t \mathbf{u}\, dt. \tag{7}$$

The second step correspond to solving

$$\frac{d\omega}{dt} = \frac{1}{Re}\nabla^2\omega \tag{8}$$

using the random walk method developed in the next section which is based on the 2D solution of the heat equation (Ghoniem & Sherman 1985), namely

$$Gr(\mathbf{x}, t) = \frac{1}{\sqrt{4\pi\nu t}} \exp(\frac{-(\mathbf{x}\cdot\mathbf{x})}{4\pi\nu t}). \tag{9}$$

These two solutions are combined to obtain the total transport of vorticity due to convection and diffusion.

2.3. NUMERICAL MODEL

In the interior domain, we discretise $\omega(\mathbf{x})$ by small area elements called vortex blobs. Each element carries a finite and invariant circulation Γ. The vorticity of a blob is smoothed according to a rapidly decreasing, radially symmetric core function $f_\delta(r)$ with a finite core radius δ. Then, the vorticity distribution can be approximated with N_V vortex blobs (N_V is the number of vortex blobs in the computational domain) by

$$\omega(\mathbf{x}) = \sum_{i=1}^{N_V} \Gamma_i f_\delta(|\mathbf{x} - \mathbf{x}_i|). \tag{10}$$

Using equation (3), the rotational velocity is approximated by

$$\mathbf{u}_\omega(\mathbf{x}_j) = \sum_{i=1}^{N_V} \Gamma_i \mathbf{K}_\delta(|\mathbf{x}_j - \mathbf{x}_i|). \tag{11}$$

where $\mathbf{K}_\delta$ is the smoothed integral kernel of velocity:

$$\mathbf{K}_\delta(\mathbf{x}, 0) = -\frac{1}{2\pi}\frac{(y, -x)}{r^2}\frac{2\pi}{\delta^2}\int_0^r r f_\delta(\frac{r}{\delta})\, dr. \tag{12}$$

In this work a Rankine core function is used.

For the potential function ϕ in equation (4), the solution is obtained using a finite-element method. Linear basis functions on triangular elements are used for the approximation of ϕ, and a Galerkin weighted-residual minimisation is employed to reduce the differential equation to a set of linear algebraic equations (Martins & Ghoniem 1993). Here, a comment on the choice of the numerical model seems to be useful. For such a complex geometry with no-slip conditions, the use of the Biot-Savart law, applied using the fast multipole methods, was not possible (because of their applicability to non-viscous flows). It seemed to be

appropriate to choose a finite-element method that is convenient to complex geometries. This reduces the consuming time to a proportional value of the number of particles N_V and N_S.

As mentioned in the previous section, the velocity must be zero at the wall. Therefore, the vorticity in the boundary region (of δ_s thickness) is discretised by N_S vortex sheets (Chorin 1978) with h as the sheet length and γ_i the unit strength. (Here, N_S is the number of vortex sheets in the numerical boundary layer).

The vortex sheets are transformed to vortex blobs and vice-versa as they cross the boundary region. The approximation for $\mathbf{u}$ is determined by:

$$\mathbf{u}(x,y) = \mathbf{u}_p(x,\delta_s) + \mathbf{u}_\omega(x,\delta_s) + \sum_{j=1}^{N_S} \gamma_j b_h(x-x_j) H(y-y_j), \tag{13}$$

where $b(x)$ is the smoothing function for vortex sheets, and $H(y)$ is the Heaviside function.

At each time step, at each control point of the wall, the spurious velocity $u(x,0,t)$ is evaluated (by equation (12)) and the corresponding circulation $\delta\Gamma = u(x,0,t)\cdot h$ is converted into N_S newly created vortex sheets of individual strength Γ_m. This procedure nullifies the otherwise non-zero slip velocity $u(x,0,t)$ at that point, and consequently mimics the correct physics of the mechanism of vorticity generation at material boundaries. More precisely on the corner points of the separator, instead of the Kutta condition, the vorticity is injected with a velocity component parallel to the upper wall with a rate:

$$\frac{d\Gamma}{dt} = \int \omega u \, dy = \left| \frac{\mathbf{u}_p + \mathbf{u}_\omega}{2} \right|^2, \tag{14}$$

where $\omega \simeq \partial u/\partial y$.

The mathematical scheme for the advection and diffusion calculations in the boundary and interior domains are the same (the viscous splitting method). For the convection step vortex sheets and vortex blobs are advected by their own local velocities.

For the diffusion step the Random Walk Method (RWM) (Ghoniem & Sherman 1985) is used. This is based on the rule that a large collection of particles undergoing Brownian motion provide a good approximation of the heat equation. Here, to increase the accuracy of the random walk method we increased the number of the vortex elements (that is, equivalent of decreasing their strength).

Of course, in this kind of high Reynolds number vortex flow, the flow is mainly dominated by convection and the effect of the diffusion is generally much less important (Mortazavi 1997). Nevertheless, a large number of particles (with smaller values of Γ_m) not only provides a better approximation of the diffusion process by the RWM (Ghoniem & Gagnon 1987, Ghoniem & Sherman 1985) but also gives a more precise discretisation of the rotational field through a greater degree of core overlap (Ghoniem & Gagnon 1987, Mortazavi 1997, Mortazavi et al. 1996). The criteria for the choice of the number of particles is related to the accuracy and the convergence of the RVM and has been separately studied by the authors (Mortazavi 1997, Mortazavi et al. 1996).

Using the identity between the Green's function of the diffusion equation and a probability density function of a random Gaussian variable, we simulate stochastically equation (9) through a two-dimensional displacement at each time step Δt using a set of independent Gaussian random numbers (η_x, η_y) with standard deviations $\sigma_{\Delta t} = \sqrt{2\nu\Delta t}$.

Finally, the total transport of vortex elements is obtained adding the two fractional contributions to the movement

$$\mathbf{x}_j^{k+1} = \mathbf{x}_j^k + L(\mathbf{u} \cdot \Delta t) + \boldsymbol{\eta}_j, \tag{15}$$

with $\boldsymbol{\eta} = (\eta_x, \eta_y)$. Here, L is the convective tranport operator (in this work, Heun's second-order method and the first-order Euler method are used for the time integration of vortex particles, respectively, in the interior and boundary regions).

The precision of the computational procedure is influenced by: the time step (Δt), the intensity of the elements (their circulation, Γ_m), the spatial discretisation values of sheets or blobs (h or δ), and the mesh size. The accuracy and numerical convergence of the scheme for complex flows, as a function of the above mentioned parameters, has been already studied by Ghoniem & Gagnon (1987), Sethian & Ghoniem (1988), Mortazavi (1997), and Mortazavi *et al.* (1996). Numerical parameter values implemented in this work are: $\Delta t = 0.05$, $\Gamma = 0.0033$ and $h = 0.05$. These parameters satisfy all necessary requirements for numerical convergence of the computational results (Mortazavi 1997, Mortazavi et al. 1996). It should be noted that the spatial choice of $h = 0.05$ is directly related to the choice of the core radius δ by $\delta = h/2$ that fulfills the spatial continuity conditions (Martins & Ghoniem 1993, Mortazavi 1997, Mortazavi et al. 1996). Furthermore, the core diameter (or the sheet length) is related to the mesh size. In our case, this numerical condition is satisfied by choosing equal values of the mesh and the sheet length. It has been shown, by comparing results with different vortex core sizes, that for a suitable range of the spatial and the time discretisation parameters (h or δ should vary as the square root of Γ_m and Δt), the solutions do not depend on the choice of vortex core size (Ghoniem & Gagnon 1987, Sethian & Ghoniem 1988, Mortazavi et al. 1996). Furthermore, these numerical convergence studies are strengthened by the experimental validations of the RVM for several high Reynolds number complex flows (Ghoniem & Gagnon 1987, Gagnon et al. 1993, Najm & Ghoniem 1991, Ghoniem & Ng 1987, Martins & Ghoniem 1993) similar to the flow studied in this work.

After a flow establishment phase, the post processing procedure and the parametric study described at the next section correspond to a sample of 600 consecutive time steps.

2.4. POST-PROCESSING PROCEDURE AND NUMERICAL VISUALISATION

Quantitative and qualitative flow visualisations are applied to identify various fluid structures and characterise their spatial dependencies. Once defined, the spatial relationship between these structures can be compared by visualising them. This visualisation is also helpful to study their generation, evolution and mutual interactions. Furthermore, the statistical significance and relevance of each class of structures, their spatio-temporal relationship and dynamical behaviour can be studied using this class of visualisation methods. This flexibility is accompanied by a huge amount of information on the structural features of the flow behaviour and so it permits us to select the statistics convenient to the description of the reproducible sequences of events. A helpful analysis of the above mentioned subjects, and particularly the strategy of turbulent flow visualisation and related data processing, is presented by Robinson *et al.* (1988).

This study is of specific interest to the case of flows with large Reynolds number ($Re = 7000$), where vortical structures have an important role in the turbulence production and in

the momentum transfer (Robinson et al. 1988). In this work, the generation of two vortex layers of opposite signs that merge from two sides of the plate, just after the separation zone, causes instabilities and deforms the eddy structures in the mixing zone (Giovannini et al. 1995). On the one hand, since Re is large, the vortical zones are very precisely defined and concentrated in sub-vortical regions. On the other hand, the analysis of complicated fluid mechanisms, e.g. "backs (velocity discontinuities)", need a powerful numerical visualisation tool. Another difficulty that must be overcome in this study are background regions of very low vorticity. The weak vortical intensity of these regions can make their influence disappear from the computational field. This elimination can be the origin of a false interpretation of the vortical behaviour. Nevertheless, the vortex method that deals directly with the rotational flow directly can easily overcome this type of problem.

3. ANALYSIS AND VISUALISATION OF NUMERICAL RESULTS

3.1. THICK PLATE: (A) AVERAGE FLOW FIELD

Average streamlines are presented in the Figure 2. A large recirculation zone, just downstream of the obstacle is observed. The flow map is essentially dominated by the external flow; nevertheless, a part of the internal jet escapes toward the exit boundary along the axis of symmetry. As the figure shows, the upper negative recirculation zone is attached to the wall, and the lower positive one is blocked between the jet flow and the upper zone. The total length of these regions is approximately equal to $2h_b$.

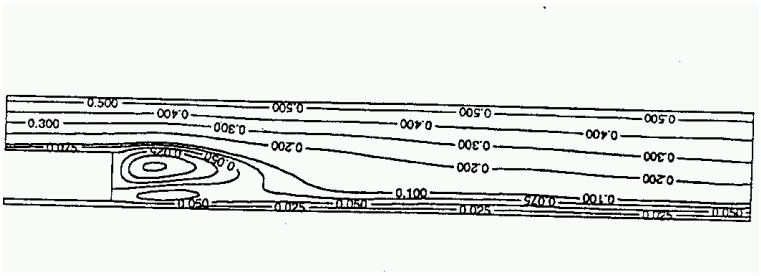

Figure 2. Average streamlines ($\Gamma = 0.0033$, $\Delta t = 0.05$ $h = 0.05$ and $Re = 7000$; thick bluff-body).

3.2. THICK PLATE: (B) INSTANTANEOUS DESCRIPTION OF THE FLOW DYNAMICS

The evolution with time of ω, the vorticity, and the integrated quantity Ψ, the stream function, are an important source of information to study the vorticity dynamics. Movie 1 and Movie 2 correspond respectively to streamlines and to the vorticity ω. Two important series of events detected in the vortex behaviour (Movie 2) concern essentially the formation and transport of eddies. This kind of visualisation shows the quasi-periodic creation of two important vortical structures: a clockwise rotating eddy at the external edge of the bluff-body (that moves towards the axis with negative circulation values), and a positive counterclockwise eddy created by the inner jet flow which has an outward motion. The

jet flow which has a momentum equal to: ρV_j^2, provides a positive circulation in the flow: $\delta\Gamma_{inj} = V_j^2 \Delta t/2$.

3.2.1. *The Formation Phase*

The mutual interaction of the jet and the external flow is the principal origin for the formation of vortical structures. It is easy to see that the upper vortical structure dominates generally the motion of the lower one. This aspect limits the growth of the vortex which resides underneath, and which finally is separated from the normal wall by a vertical upside motion. Furthermore, when these structures come together to create an instantaneous region with twice the length of the average recirculation zone, a breakdown with the creation of a vortex pair is observed. These events are described as follows: the convergent motion of these two eddies creates for a short time a composite vortical structure and initiates progressively the vortex shedding. Later, a separation of these eddies from each other occurs, approximately at the same time that the bigger external vortex separates from the bluff-body wall. The reason for the separation of the external eddy from the bluff-body seems to be the transverse creeping motion of the inner eddy toward the external edge, on the wall surface (close to time-step 510). Once the upper flow begins to block the development of the inner jet, the inner flow breaks down into two portions (T2 & T3, Figure 3), one part taking a backward motion and progressing along the normal wall, the other one growing behind the external flow and separating this flow in two parts (T4 & T1); this effect due to the internal flow creates a blockage in front of the external vortex and divides the vortex also in two sections (Figure 3). The two above mentioned separations, which take place successively, are the principal causes of the vortex shedding and eddy structure pairs generation. The vortex pairs created are immediately injected in the flow. Few steps later, the rest of the inner structure separates from the wall, to be replaced by two new vortical structures which form in front of the bluff-body (the separated lower vortex is moving in fluid following two general behaviours: either it is advancing along the axis toward the exit boundaries, or it is propagating in the domain closer to the upper wall). This procedure represents a quasi-periodic sub-cycle which occurs approximately every 200 steps, in the statistically steady regime. Nevertheless, in a high Reynolds number flow this periodicity is never fixed with an identical repetition of fluid motions (e.g. sometimes, during the creation of two vortex pairs, several very small structures with smaller circulations are formed and dispersed along the axis of symmetry); however, it constitutes a capability of prediction of global fluid macro-structure behaviour (e.g., vortical structures motion and interactions) during time.

3.2.2. *The Transport Phase*

Once imparted into the flow, vortex pair structures have various trajectories (Movie 2). Either they are attracted toward the upper wall, corresponding to the so-called mechanism of dipole ejection, with the negative vortex that is advancing in the vicinity of the wall downstream of the positive vortex, or they are accelerated attaining upstream eddies and creating more complex structures that contain several vortices mixing and spinning around each other. Also, other behaviours can be detected: some particles of the negative structure spin around the positive vortex and remains of that structure then accelerate toward the exit boundary across the upper wall (e.g., step 680-730, Movie 2). It is apparent that, globally, negative structures move faster than positive vortices (steps 700-730, 560-600,

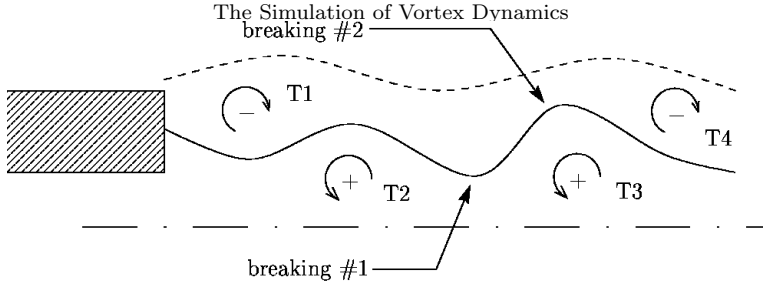

Figure 3. Eddy formation mechanism ($\Gamma = 0.0033$, $\Delta t = 0.05$ $h = 0.05$ and $Re = 7000$; thick bluff-body).

Movie 2). As shown in Movie 2, some eddy agglomerations are formed from smaller particle patches which advance in time translating and spinning around each other. However, some isolated patches with individual behaviour are noticeable in different parts of the flow. These isolated agglomerations, that were previously detached from the large eddies, correspond to low-vorticity regions. Later, they can reattach again to other large-scale structures or continue their individual movement.

3.3. THICK PLATE: (C) PRESSURE FIELD

The visualisation of this field allows us to study the vortex pressure-velocity relationship (e.g., the relationship between low pressure regions and vorticity or the high pressure regions distribution versus those of the vortical structures). Vortical structures are concentrated in low pressure regions (Saffman 1993), but some low pressure regions (i.e., regions not-elongated (Robinson et al. 1988)) represent other fluid interactions (local accelerations).

Snapshots of the pressure fields with corresponding vortical streamlines (Figure 4) enlighten the strong correlation between vortical structures of opposite signs and the corresponding induced pressure. Elementary effects, resulting essentially from inviscid interactions, can be isolated and explained as follows (Mortazavi 1997):

(1) Under-pressure inside the vortical core of the structure due to the presence of vorticity and to its rotation.
(2) In the neighbourhood of the upper wall and the axis of symmetry, the effects are similar. We notice the presence of a depression in the right hand of the structure due essentially to its movement. This dynamical effect is recovered by the unsteady term of the Bernoulli equation (being the total velocity potential). The image effect contributes also to the depression.
(3) Between two structures of opposite signs, as encountered in our geometry, we visualise an under-pressure.

3.4. THIN PLATE: (A) AVERAGE FLOW FIELD

Figure 5 shows the evolution of average streamlines for the thin bluff-body. The recirculation zone, which does not present the complex features of the previous case, is short

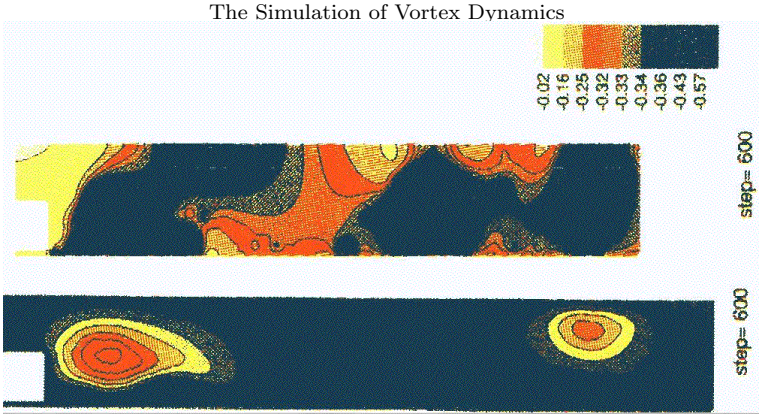

Figure 4. Vorticity contour plot (top) and corresponding pressure field (bottom) ($\Gamma = 0.0033$, $\Delta t = 0.05$, $h = 0.05$ and $Re = 7000$; thick bluff-body).

and streamlines become rapidly parallel to one another at the downstream of the channel. This effect is due to the smaller thickness of the obstacle that permits two flow-streams to join easily and rapidly together downstream of the obstacle. Nevertheless, the existence of two recirculation zones of opposite sign constitutes the main resemblance between the thin bluff-body flow and the previous thicker one; the positive zone being blocked between the inner jet and the negative recirculation zone. The total length of these recirculation regions is again equal approximately to $2h_b$.

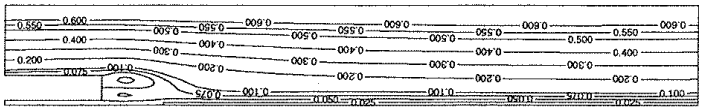

Figure 5. Averaged streamlines ($\Gamma = 0.0033$, $\Delta t = 0.05$, $h = 0.05$ and $Re = 7000$; thin bluff-body).

Figure 6 compares average streamwise velocity profiles for three different obstacle thicknesses: $H = 0.3$, 0.4 and 0.5, but at the same normalised distances x/h_b, where x corresponds to the distance of the section from the bluff-body base. As shown in this figure, velocity profiles $U(y)$ normalised respectively by V_e for the velocities and by h_b for the distances to the axis exhibit equivalent minimal velocities and wake gradients behaviour. So, average streamwise velocity values and distributions are geometrically similar and vary as a function of bluff-bodies thickness.

3.5. THIN PLATE: (B) INSTANTANEOUS DESCRIPTION OF THE FLOW DYNAMICS

For the thin bluff-body the instantaneous evolution of the flow field is described in two stages, as follows (see Movie 3).

3.5.1. *The Formation Phase*

This stage can be summarised by the following observations:

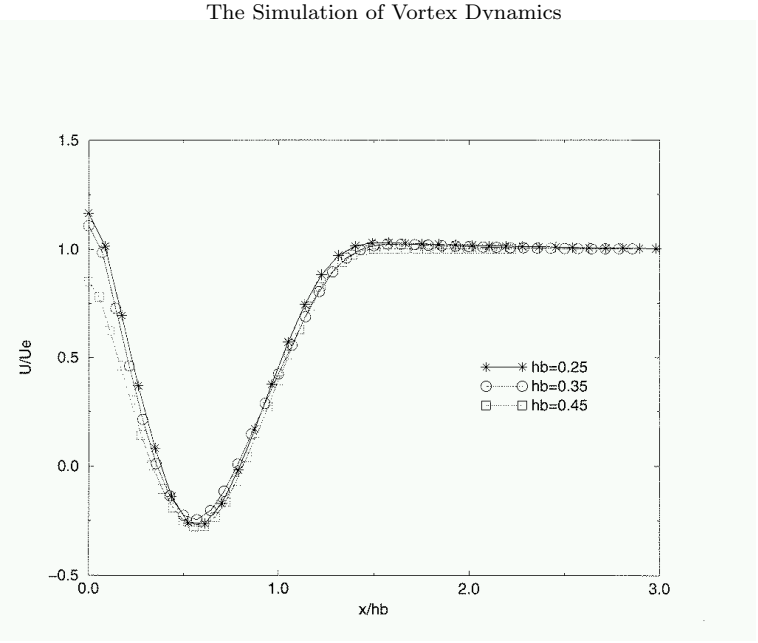

Figure 6. Normalised averaged streamwise velocity profiles $U/V_e = f(y/h_b)$ for the three bluff-bodies for the same relative distance x/h_b from the bluff-body base.

(1) Formation of a large eddy structure, which rotates in the clockwise direction, on the upper edge of the bluff-body due to the roll-up of the external flow boundary layer. During this part of the cycle, some of the inner-jet fluid escapes along the centerline.
(2) Formation of a smaller eddy, which rotates in the anticlockwise direction, on the inner edge of the bluff-body due to the roll-up of the inner jet boundary layer. This eddy remains confined by the external flow.
(3) Separation of the upper flow eddy from the plate wall as the jet-eddy fills the gap between it and the plate face.
(4) The external flow confines the jet flow and cuts it in two parts; the separation of the second part of the jet eddy is then entrained by the external flow while the latter is flowing downstream.
(5) The upward expansion of the inferior structure which imposes a rupture in the upper vortex and affects its later shedding.
(6) Pairing of these two eddies as they flow downstream.

3.5.2. *The Transport Phase*

The newly formed vortex pair structure follows the flow approaching the upper boundary of the domain. The negative eddy adheres rapidly to the upper wall and the positive one shows the same behaviour later. The mechanism of dipole ejection is visible, e.g., for steps 690-750. This scenario is sometimes perturbed by eddies that turn around each other forming larger composite structures with an increasing rate of dispersion. Furthermore, convected vortex pair structures advance more rapidly and form more concentrated struc-

tures in the flow than in the previous case. Another significant difference between the two cases is that for the thin bluff body the length and time of vortex shedding is proportionally shorter compared to the thick bluff body.

3.6. MONITORING POINTS AND FREQUENCY ANALYSIS

To complete this study we have chosen several monitoring points trying to detect their individual frequencies for both cases. This detection is made on 600 successive steps at the established phase for the streamwise velocity values. The dominant frequency for a point at the recirculation zone for the thin obstacle ($f = 0.67$) was larger than for the thick one ($f = 0.49$); this higher value corresponds to a faster mechanism of eddy formation and vortex shedding. Using the corresponding eddy size and computed average velocity at that point, a Strouhal number equal to 0.24 is calculated for both cases. This value agrees with the Strouhal number observed in other experimental and numerical studies concerning flows past bluff-bodies inside channels (Kenworthy 1971, Ho & Huerre 1984, Martins & Ghoniem 1987). For other points, close to the shear layers between the recirculation zone and the main streams we obtain a Strouhal number equal to 0.17–0.18. This result is also in good agreement with the *universal* Strouhal number (St=0.17) achieved as a reference value in bluff-body flows (Martins & Ghoniem 1987, Calvert 1967). In this case the obstacle thickness is used as the reference length. Finally, for several monitoring points we compared the instantaneous velocity modulus during 800 successive time steps. The thin plate generates a faster velocity pulsation with larger intensities.

3.7. EFFECT OF THE VELOCITY RATIO

This comparison is done using two different entry velocity ratios corresponding to $V_j/V_e = 0.5$ and $V_j/V_e = 2.0$ (V_e is the external entry velocity and V_j represents the jet entry velocity). For the second velocity ratio, to satisfy the Courant timestep restriction (Mortazavi et al. 1996), the following parameters are used ($\Delta t = 0.025$, $\Gamma = 0.0033$ and $h = 0.05$). For larger values of the external flow we observed complex interactions of the large eddies essentially dominated by the main stream. Nevertheless, the evolution of these complex vortex interactions is predictable by two principal series of quasi-cyclic events in the flow map. For the second case study (larger jet velocities) we observed a reasonable decrease in the vorticity formation that leads directly to a decrease of the interactions between vortical structures of internal and external flow.

3.7.1. *(a) First Case* $V_j/V_e = 0.5$

Movie 4 shows the evolution of vortical structures between steps 650 and 1500. One can easily observe that the inner jet is completely blocked by the external flow which stops its motion along the axis. Therefore, the jet flow that is the origin of the creation of the positive vorticity, either goes up on the vertical face of the bluff-body toward its upper edge, or is dispersed downstream of the obstacle intensifying the shedding procedure of negative structures (steps 800, 1150, 1300 and 1450). This positive eddy that is extended along the wake of the obstacle is also broken in two parts by the external flow. The shedding of large negative vortical structures is then followed by the separation of an ensemble of positive vortices (broken in two parts). These two large eddy structures, which show a reciprocal

progressive creeping motion, are convected together in the flow (e.g., steps 700, 850, 1050, 1200, 1350 and 1500).

These shedding events are repeated approximately every 200 steps in a quasi-cyclic manner. At times a kind of artificial blockage is created by a part of an eddy structure, just downstream of the formation region, which waits for the joining of some other detached eddies from the formation region. Larger eddies due to this process are then convected in the flow (e.g., steps 800, 1150 and 1300). An important contribution to these large vortical structures are from small positive vortex patches which often orbit around the large negative structures until they exit the domain.

Average streamlines (Figure 7) confirm these observations. Two principal recirculation zones are visualised. The first one is a small recirculation zone just attached to the obstacle which depends essentially on the interaction of the jet with the solid wall. A second large recirculation zone can be attributed directly to the formation and shedding of large eddy structures before the transport phase.

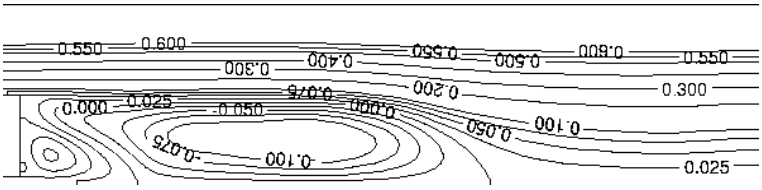

Figure 7. Average streamlines ($V_j/V_e = 0.5$, $\Gamma = 0.0033$, $\Delta t = 0.025$, $h = 0.05$, $Re = 7000$; thick bluff body)

3.7.2. *(b) Second Case ($V_j/V_e = 2.0$)*

In this case we observed a restriction of merging and mixing of eddies. This is directly related to the weaker energy level of the structures.

Movie 5 confirms this observation. The jet flow maintains its individuality across the axis of symmetry; and the influence of the negative structures (that have an injection rate of circulation four times smaller) on the jet flow is weak. However, the accumulation of the eddies issued from the upper flow, just on the top side of the jet flow, permits the formation of a large negative structure (step 700) and its interaction with neighbouring positive vortices results in a mutual simultaneous shedding of positive and negative structures (step 750). The *roll up* behaviour of the negative vortex around the positive eddy and its development by the last one can be considered as a particular case of the *eddy suction* phenomenon. Moving toward the exit boundary of the domain, the two structures remain always separated and grow gradually. The negative eddy that continues to grow blocks the channel flow by reaching the top of it, and the positive structure is diluted slightly (step 950-1100).

A different behaviour is noticed for negative vortices that are not sufficiently energetic to break down positive structures. Therefore, these structures continue systematically their motion along the axis of symmetry (step 1100). A portion of the particles issued from the jet flow rise along the bluff body's vertical wall, but this phenomenon does not generate a direct shedding consequence. Essentially, positive and negative structures which advance and develop progressively in the channel, remain almost parallel together. They do not have

enough dynamical energy to mix and merge and therefore, no dipole creation is noticed in the flow. The higher velocity of the jet flow and its larger momentum seems to be at the origin of this behaviour.

Figure 8 (average streamlines) confirms these remarks. The recirculation zone is not only longer than in other cases ($x_r/h_b \simeq 3.5$), but also is neighboured near its bottom by a large low circulation region: on the one hand, the jet claims this low circulation area, and on the other hand it pushes upward the recirculation zone.

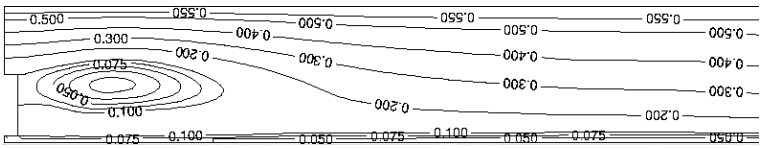

Figure 8. Average streamlines ($V_j/V_e = 2.0$, $\Gamma = 0.0033$, $\Delta t = 0.025$, $h = 0.05$, $Re = 7000$; thick bluff body)

4. CONCLUSION AND PERSPECTIVES

In the present work, we used the Random Vortex Method to study the flow downstream of a bluff-body geometry. The effect of the obstacle thickness and the inlet velocity ratio on the physics of the flow and the vortex dynamics was analyzed. The variable of most interest, ω, is directly connected to the vortical structures; hence, the computational task is adapted and refined in regions of high vorticity, where vortex shear events, the physics of vorticity generation, and the dynamics of evolution are quite well depicted by this vortex method.

Visualisation techniques are applied to achieve a better understanding and generalisation of instantaneous flow events. They allow us to classify the various steps of the fluid flow. The post processing of the results occurs during a long time sequence compared to the evolution scale of the largest eddies. The simultaneous presentation of animated 2D plots of scalar variables like stream-function and vorticity allows us to understand the significant interactions and later classify the elementary corresponding events.

The thick and thin bluff-body geometries simulated using the vortex method are characterised by a strong interaction of coherent structures of opposite signs. We chose a velocity ratio between two streams equal to one in order to increase the topological interest of the phenomenon. Two vorticity layers on the two edges of the separation feed positive and negative vortical structures that grow, interact, and then merge inside the channel as their length scale increases. In both cases simulated, the dynamics is governed initially by the shedding of large vortex eddies from the inner and outer sides of the bluff-body. Mixing between the two streams is enhanced by the merging of these eddies downstream of the bluff-body and the formation of composite structures. The entrainment mechanism is the merging of the two eddies. We found that the level of fluctuations increases and the frequency of shedding decreases with larger thickness ratios. The evolution of these complex vortex interactions is predictable by two principal series of quasi-cyclic events in the flow map. The formation and shedding procedure of eddy structures occur approximately on a cycle of dimensionless period equal to about 10. For both structures, these events lead

to the creation of vortex pairs which evolve and advance in the flow, with various (and different) behaviours as function of the bluff-body thickness. For the thin bluff-body, we detected a better conservation of the identity of the eddy structures along their trajectory in the flow. This effect seems to be due to their smaller size and faster transport in the flow. The influence of differential inlet velocity on the evolution and interaction of vortical structures for two opposite cases is studied. In both cases, the flow mechanisms are essentially dominated by the flow having the largest inlet velocity value.

The combination of this vortex method with the post-processing dynamic visualisation software makes this a powerful approach in order to understand, analyze and characterise unsteady vortical flows.

5. ACKNOWLEDGEMENTS

The authors acknowledge Professor P. Micheau for valuable suggestions and constructive remarks during the course of this work. Furthermore we are very grateful to Professor A. Ghoniem for his participation at the beginning of this study. The authors are deeply indebted to the invaluable help of Sandrine Layrisse and Philippe Depouilly (IMB Bordeaux) for the internet adaptation of this work. Most of the calculations and image processing were performed at the *Institut du Developpement et des Resources en Informatique Scientifique (IDRIS)* of *CNRS-Orsay*, France.

References

1. Blot, F., Giovannini, A., Hebrard, P. & Strzelecki, A. (1989) Flow Analysis in a Vortex Flowmeter: An Experimental and Numerical Approach, in *Turbulent Shear Flows*, Stanford, August 1989.
2. Calvert, J.R. (1967) Experiments on the Low-Speed Flow Past Cones, *J. Fluid Mech.*, **27**, 273–289.
3. Choi, Y., Humphrey, J.A.C. & Sherman, F.S. (1988) Random Vortex Simulation of Transient Wall-Driven Flow in a Rectangular Enclosure, *J. Comp. Phys.*, **75**, 359–383.
4. Chorin, A.J. (1973) Numerical Study of Slightly Viscous Flow, *J. Fluid Mech.*, 273–289.
5. Chorin, A.J. (1978) Vortex Sheet Approximation of Boundary Layers, *J. Comp. Phys.*, **27**, 428–442.
6. Gagnon, Y., Giovannini, A. & Hebrard, P. (1993) Numerical Simulation and Physical Analysis of High Reynolds Number Flows behind Sudden Expansions, *Phys. Fluids*, **A5**, 2377-2389.
7. Gagnon, Y. & Huang, W. (1993) Fast-Vortex Method for the Simulation of Flows inside Channels with and without Injection, *Int. J. Thermal Fluid Sc.*, **2** 1–11.
8. Ghoniem, A.F., Chorin, A.J. & Oppenheim, A.K. (1982) Numerical Modeling of Turbulent Flow in a Combustion Tunnel, *Philo. Trans. Roy. Soc. London*, Series A, **304**, 303–325.
9. Ghoniem, A.F., & Sherman, F.S. (1985) Grid-Free Simulation of Diffusion using Random Walk Methods, *J. Comp. Phys.*, **61**, 1–37.
10. Ghoniem, A.F. & Gagnon, Y. (1987) Vortex Simulation of Laminar Recirculating Flows, *J. Comp. Phys.*, **68**, 346–377.
11. Ghoniem, A.F. & Ng, K.K. (1987) Numerical Study of the Dynamics of a Forced Shear Layer, *Phys. Fluids*, **30**, 706–721.
12. Giovannini, A., Mortazavi, I. & Tinel, Y. (1995) Numerical Flow Visualisation in High Reynolds Numbers using Vortex Method Computational Results, *ASME Summer Meeting*, **FED 218**, 37–43.
13. Ho, C.M. & Huerre, P. (1984) Perturbed Free Shear Layers, *Ann. Rev. Fluid Mech.*, **16**, 365–424.

14. Kenworthy, J.S. (1971) The Flow and Mixing in Double Concentric Jets, *Ph.D. Thesis*, University of Sheffield, 1971.
15. Martins, L.F. & Ghoniem, A.F. (1993) Simulation of the Non-Reacting Flow in a Bluff-Body Burner: Effect of the Diameter Ratio, *J. Fluids Eng.*, **115**, 474–484.
16. McCracken, M.F. & Peskin, C.S. (1980) A Vortex Method for Blood Flow through Heart Valves, *J. Comp. Phys.*, **35**, 183–205.
17. Mortazavi, I. (1997) Methode Hybride Vortex-Elements Finis: Etude de la Convergence Numerique, Caracterisation et Analyse d'un Ecoulement Complexe, *Ph.D. thesis*, University of Lille 1, January 1997.
18. Mortazavi, I., Micheau, P. & Giovannini, A. (1996) Numerical Convergence of the Random Vortex Method for Complex Flows, *European Series in Applied and Industrial Mathematics*, **1**, 571–589.
19. Najm, H. & Ghoniem, A.F. (1991) Numerical Simulation of the Convective Instability in a Dump, *AIAA J.*, **29**, 911–919.
20. Robinson, S.K., Kline, S.J. & Spalart, P.R. (1988) Quasi-Coherent Structures in the Turbulent Boundary Layer: Part II. Verification and New Information from a Numerically Simulated Flat-Plate Layer, *Zoran P. Zaric: Memorial International Seminar on Near-Wall Turbulence*, Dubrovnik, 218–242.
21. Saffman, P.G. (1993) Vortex Dynamics, Cambridge University Press, Cambridge, 1993.
22. Sethian, J.A. (1984) Turbulent Combustion in Open and Closed Vessels, *J. Comp. Phys.*, **54**, 425–456.
23. Sethian, J.A. & Ghoniem, A.F. (1988) Validation Study of Vortex Methods, *J. Comp. Phys.*, **74**, 283–317.
24. Summers, D.M., Hanson, T. & Wilson, C.B. (1985) A Random Vortex Simulation of Wind Flow over a Building, *Intern. J. Num. Meth. Fluids*, **5**, 849–871.

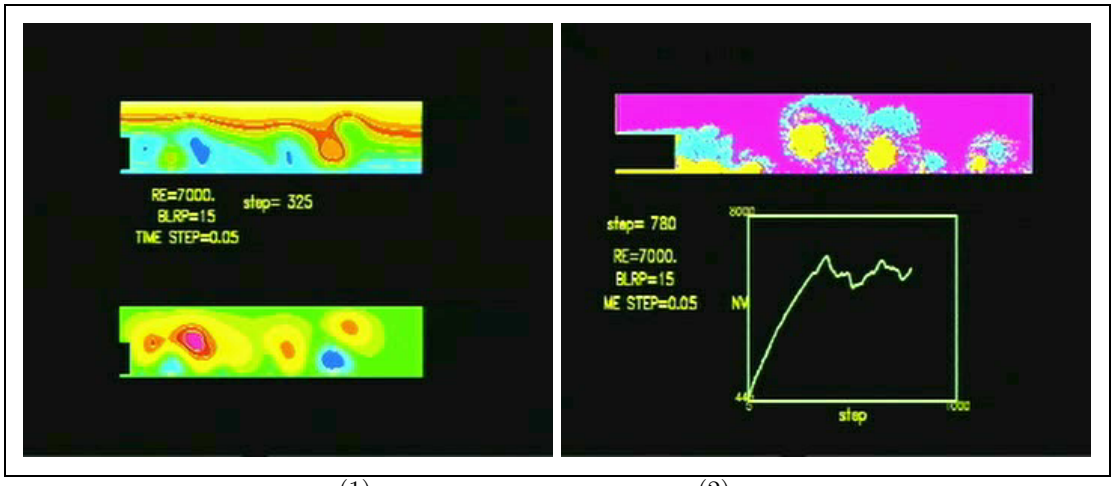

(1) (2)

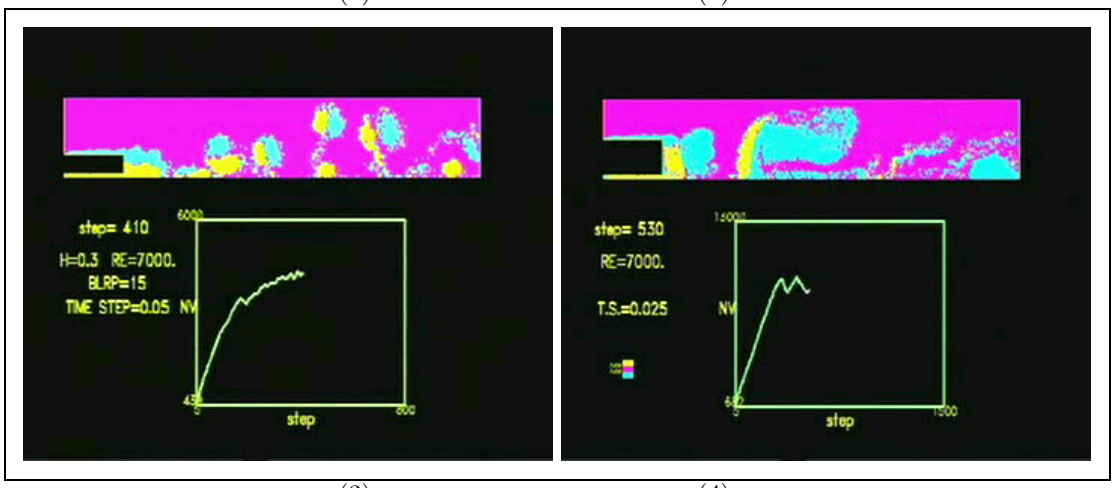

(3) (4)

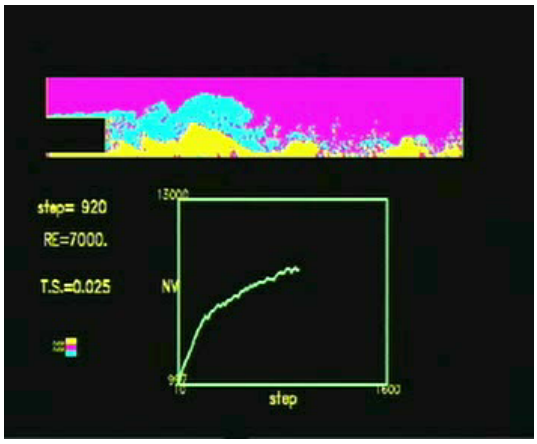

(5)

Stills from movies 1 through 5.